Macromolecules

pubs.acs.org/Macromolecules Article

The Impact of Polymerization Chemistry on the Mechanical Properties of Poly(dimethylsiloxane) Bottlebrush Elastomers

Brandon R. Clarke,[§] Hyemin Kim,[§] Mark Ilton,* James J. Watkins,* Alfred J. Crosby,* and Gregory N. Tew*

Cite This: *Macromolecules* 2022, 55, 10312–10319 Read Online

ACCESS | Metrics & More | Article Recommendations | Supporting Information

ABSTRACT: We compare the low-strain mechanical properties of bottlebrush elastomers (BBEs) synthesized using ring-opening metathesis and free radical polymerization. Through comparison of experimentally measured elastic moduli and those predicted by an ideal, affine model, we evaluate the efficiency of our networks in forming stress-supporting strands. This comparison allowed us to develop a structural efficiency ratio that facilitates the prediction of mechanical properties relative to polymerization chemistry (*e.g.*, softer BBEs when polymerizing under dilute conditions). This work highlights the impact that polymerization chemistry has on the structural efficiency ratio and the resultant mechanical properties of BBEs with identical side chains, providing another "knob" by which to control polymer network properties.

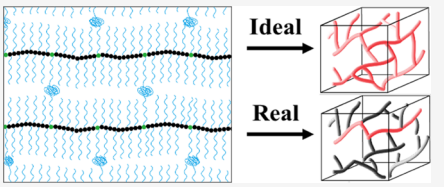

INTRODUCTION

Bottlebrush networks are receiving increased attention due to the unique architectural possibilities afforded by the side chains densely grafted upon strands of the network.[1−14] The high local density of side chains extends the backbone and produces networks where the strands are rigid cylinders that are less likely to form physical entanglements, resulting in supersoft materials with moduli similar to biological tissue without the need for solvent swelling.[4,7] Major architectural parameters of bottlebrush networks are n_g, n_{sc}, and n_x—the degree of polymerization between side chains, of side chains, and between crosslinks, respectively (Figure 1). This diversity of parameters allows for bottlebrush elastomers (BBEs) to have a wide degree of tunability, enabling the design of solvent-free materials with moduli ranging from 10^2 to 10^6 Pa.[7,15,16]

It is highly desirable to "map" the architectural parameters of BBEs such that materials of tunable elasticity, modulus, adhesion, and failure behavior can be designed.[17−20] Modern advances in network theory allow for increasingly accurate predictions of network bulk properties (*e.g.*, modulus, adhesion, fracture).[9,10,20−29] These predictions are anchored by an evolving understanding of the underlying molecular parameters associated with network materials. Models developed this way are often improved through correlation of molecular structure and bulk mechanical properties.[30−37] This approach typically entails developing more accurate ways to estimate the number and type of molecular defects within the network.[25,38−41] Despite these recent advancements, it remains difficult to predict the mechanical properties of BBEs specifically due to their unique molecular structure.

Herein, BBEs with identical side chains—n_{sc} = 14 poly(dimethylsiloxane)—but different backbones—poly(norbornene) and poly(methyl methacrylate)—are compared to evaluate the impact of network formation chemistry on the mechanical properties of polymerized elastomers. These

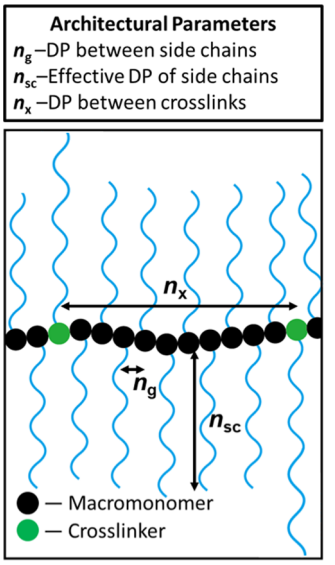

Figure 1. Schematic depiction of a representative bottlebrush elastomer, highlighting the most important architectural parameters of its molecular structure.

Received: June 28, 2022
Revised: September 19, 2022
Published: November 15, 2022

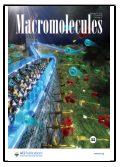

https://doi.org/10.1021/acs.macromol.2c01332
Macromolecules 2022, 55, 10312−10319

backbones were chosen because ring-opening metathesis polymerization (ROMP) and free radical polymerization (FRP) are two of the most common methods to produce bottlebrush polymers. The two chemistries differ significantly with respect to chain growth mechanisms, backbone dispersities ($Đ$), propagation rates (k_p), growing chain lifetime, as well as the extent and type of chain transfer reactions (Figure 2).[42−44] These different chemistries are expected to produce BBEs with different molecular topologies, including defects, that affect their mechanical properties.

Ring-Opening Metathesis Polymerization	Free Radical Polymerization
Living Polymerization	Chain Polymerization
$Đ$ = 1.1-1.5	$Đ$ > 1.5
$k_p \approx 10^{-3}$	$k_p \approx 10^{2}$
Relatively Long Chain Lifetime	Short Chain Lifetime
Limited Chain Transfer	Chain Transfer

Figure 2. Comparison of the ring-opening metathesis polymerization (ROMP) and free radical polymerization (FRP) chemistries. The two chemistries differ significantly in mechanism, thermodynamics, and kinetics.

We applied Dobrynin and co-workers' predictive model for BBE modulus to introduce the structural efficiency ratio (ρ_{s*}/ρ_s;SER), a comparison of the number density of stress-supporting strands in an experimentally prepared BBE (ρ_{s*}) to the number density of stress-supporting strands in an affine model BBE (ρ_s). Through this SER, the degree to which imperfections alter the molecular structure of our elastomers was evaluated. This analysis illustrated that (1) the ROMP chemistry produces stress-supporting strands less efficiently than the FRP chemistry, (2) the use of solvent during FRP leads to the production of samples with a lower SER, and (3) ROMP samples have loss moduli and loss tangents of greater magnitude than FRP samples due to their lower SER. Demonstrating that the chemistry used to grow the BBE significantly impacts the resulting mechanical properties expands the materials' design opportunities.

EXPERIMENTAL SECTION

ROMP Bottlebrush Elastomer Synthesis. ROMP BBEs were synthesized by polymerizing norbornene-functionalized macromonomers (250 mg) with varied amounts of crosslinker (Scheme S.1). The ROMP BBEs were all polymerized using Grubbs' second-generation catalyst (Sigma) at an M:I ratio of 1000. For a typical reaction, the macromonomer and crosslinker were first dissolved in 1 mL of dried dichloromethane (DCM) in a 20 mL vial before adding 1 mL of catalyst/DCM solution. The reaction was allowed to run overnight before being quenched with three drops of ethyl vinyl ether (EVE, Sigma). An analogous bottlebrush polymerization was performed in a round-bottom flask in 20 mL of dried DCM with no crosslinker added to the reaction (Scheme S.2). The synthesized bottlebrush polymer was characterized by multi-angle light scattering (MALS).

FRP Bottlebrush Elastomer Synthesis. Monomethacryloxypropyl-terminated poly(dimethylsiloxane) (macromonomer; MCR-M11, Gelest) and methacryloxypropyl terminated poly-

Scheme 1. General Polymerization Schemes for (Top) the Ring-Opening Metathesis Polymerization of Norbornene-Functionalized Macromonomers Using Grubbs' Second-Generation Catalyst and (Bottom) the Free Radical Polymerization of Methacrylate-Functionalized Macromonomers Using Photopolymerization[a]

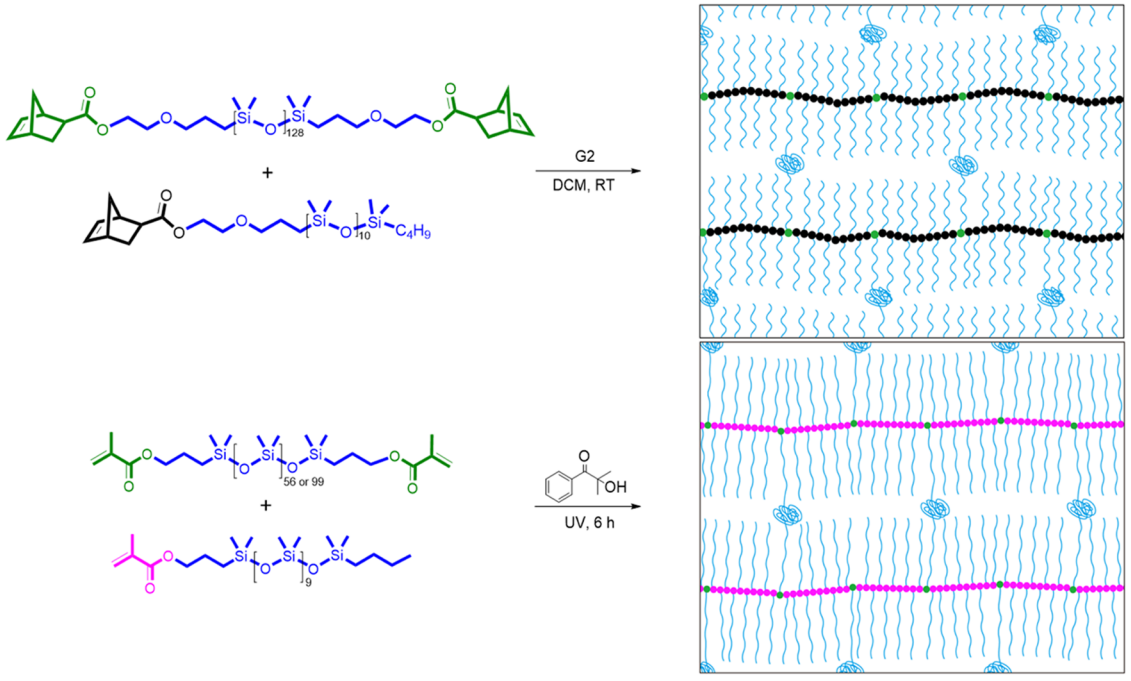

[a]The mol % crosslinker content of each of the networks is varied (n_x = (2 × mol % XL)$^{-1}$). The network schematics on the right are designed to scale, considering the length of the side chains (<R_{sc}>), the length of network strands (<R_{n_x}>), monomer volume, and the effective Kuhn length. Refer to the SI for details on these calculations. Our ROMP systems have less extended side chains (2.38 nm) than our FRP systems (2.69 nm) due to the different bottlebrush regimes they belong to (SBB and SSC, respectively).

https://doi.org/10.1021/acs.macromol.2c01332
Macromolecules 2022, 55, 10312−10319

(dimethylsiloxane) (crosslinker; DMS-R18, and DMS-R22, Gelest) were passed through basic alumina to remove any inhibitor present. FRP BBEs were all polymerized with 1.1 mol % photo-initiator (2-hydroxy-2-methylpropiophenone, Darocur 1173, BASF), and varied amounts of crosslinker. For a typical reaction, macromonomer and crosslinker were stirred with 1.1 mol % Darocur before being injected into a 40 mm diameter circular mold. Reaction mixtures were UV-cured for 6 h under N_2 with a high-pressure ultraviolet lamp (USH508SA, Ushio, 6.1 mW/cm^2 at 365 nm). An analogous bottlebrush polymerization was performed with no crosslinker added to the reaction (Scheme S.2). The synthesized bottlebrush polymer was characterized by multi-angle light scattering (MALS).

Proton Nuclear Magnetic Resonance (^{1}H-NMR). ^{1}H-NMR was used to determine the successful synthesis of macromonomer materials (Figures S.2 and S.3). ^{1}H-NMR spectroscopy was performed using a Bruker Advance 500 MHz NMR spectrometer with $CDCl_3$ as a solvent.

GPC and MALS. GPC was performed using an Agilent Technologies 1260 Infinity series system with two 5 μm mixed-D columns, a 5 μm guard column, a PL Gel 5 μm analytical Mixed-D column, and an RI detector (HP1047A); dried tetrahydrofuran (THF) was used as the eluent with a flow rate of 1.0 mL/min; polystyrene standards were used for the calibration. The dispersities ($Đ$) and molecular weights (M_w) of each macromonomer and crosslinker were measured using THF-GPC (Figures S.1 and S.4). MALS was performed in THF + 1 vol % triethylamine (TEA) using two Polymer Laboratories 10 μm mixed-B LS columns connected in series with a Wyatt Technologies DAWN EOS MALLS detector and an RI detector at a flow rate of 1.0 mL/min. MALS was used to determine the M_w of synthesized bottlebrushes, with an eluent of THF and 1% TEA.

Indentation with a Texture Analyzer. Force/displacement data were collected using a TA.XT Plus Texture Analyzer from Texture Technologies. Networks were indented with a 2 mm diameter probe at a loading rate of 0.01 mm/s to a force of 20 mN, whereupon the probe retracted at an unloading rate of 0.01 mm/s. The probe was cleaned with acetone between runs. Force/displacement data were analyzed using eq 1[45]

$$E_o = \frac{3}{8a}\frac{\Delta P}{\Delta \delta}\left\{1 + 1.33\frac{a}{h} + 1.33\left(\frac{a}{h}\right)^3\right\}^{-1} \quad (1)$$

where E_o is the apparent elastic modulus, P is the load applied, a is the radius of the indentation probe, δ is the displacement of the probe, and h is the thickness of the sample. An example force/displacement curve is available as Figure S.5. A Poisson's ratio of 0.5 is assumed for these calculations.

Dynamic Mechanical Analysis (DMA). Networks were cut into either 8 or 13 mm circles with a circular punch and placed within the compression clamps of a Discovery DMA 850 from TA Instruments. Samples were tested at room temperature, sweeping a frequency range of 0.1−100 Hz at a strain amplitude of 1% with a preload force of 0.1 N. The sample stage was cleaned with isopropyl alcohol between samples.

RESULTS AND DISCUSSION

Bottlebrush Elastomer Synthesis. Norbornene-functionalized PDMS macromonomers were polymerized using ROMP utilizing Grubb's second-generation catalyst, while methacrylate-functionalized PDMS macromonomers were polymerized using photo-initiated FRP (Scheme 1). The length of the side chains in both cases was n_{sc} = 14, similar to the side chains used in a number of previous publications.[4,7,12,15,46,47] The degree of polymerization between crosslinks (n_x) was altered to produce BBEs of varied modulus with gel fractions greater than 85% (Figure S.6). While the length of the PDMS crosslinker was varied for FRP samples, indentation showed that the length of the crosslinker had no effect on network modulus (Figure S.7).

The BBE schematics in Scheme 1 are drawn to scale for representative n_x = 10 elastomers formed from ROMP and FRP. Special care was taken to consider the end-to-end distance of the side chains ($<R_{sc}>$), the end-to-end distance of network strands ($<R_{n_x}>$), differences in monomer volume, and the effective Kuhn length of each system. Details on the calculation of these parameters can be found in the SI. Consideration of $<R_{n_x}>$ is especially interesting, as it provides information beyond "n_x = 10" to conceptualize the physical differences between our ROMP and FRP networks (3.06 nm and 2.78 nm, respectively) and has not been reported elsewhere.

Bottlebrush Elastomer Modulus. Following extraction of unreacted macromonomer, the quasi-elastic apparent modulus (E_o) of the ROMP and FRP samples was determined via indentation using a texture analyzer (Figure 3). As expected of

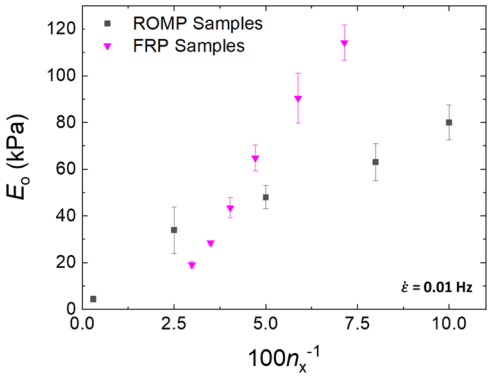

Figure 3. Plot of quasi-elastic structural modulus values obtained for ROMP samples (black) and FRP samples (magenta). Sample data are plotted as an average of sample measurements with error bars representing one standard deviation. The average strain rate at which the samples were measured is 0.01 Hz. The x-axis is represented as $100/n_x$ for ease of reference.

elastomeric materials, both ROMP and FRP samples displayed a direct, linear relationship between n_x^{-1} and E_o.[4,9,10,48] Samples produced via FRP were stiffer at low n_x values than analogous ROMP samples but also declined in E_o more sharply than ROMP samples as n_x increased. Notably, ROMP samples were able to access a region of high-n_x materials that FRP samples were not, with an n_x of 333 achieved for ROMP samples, while FRP samples were unable to reach an n_x of 50.

While previous studies by Sheiko and co-workers indicated that FRP samples should be capable of reaching n_x values of 600, we found that our samples became too weak to manipulate after n_x = 34.[4,47] Furthermore, our FRP samples were able to achieve an $E_o \sim$ 30 kPa at n_x = 34, a value not reached until n_x = 67 in Sheiko and co-workers' studies.[4,47] It should be noted that Sheiko and co-workers' BBEs were polymerized using solvent while our FRP was performed solventless. For ROMP, our n_x = 333 sample had an E_o of 4.4 kPa, comparable to an n_x = 400 sample produced by Sheiko and co-workers (2.9 kPa), illustrating the potential of ROMP samples to become even softer than FRP samples at higher n_x values (ROMP BBEs can be made at n_x = 1000 with an $E_o \sim$ 1 kPa, not shown here).

https://doi.org/10.1021/acs.macromol.2c01332
Macromolecules 2022, 55, 10312−10319

Modeling Elastic Modulus. To effectively compare the quasi-elastic modulus (E_o) of our BBEs to that of ideal BBEs, it was first essential to prepare a graft-copolymer phase diagram and determine whether our materials belonged to the comb, rodlike side chain (RSC), stretched backbone (SBB), or stretched side chain (SSC) regimes.[49] While we use the nomenclature described by Dobrynin et al. in this study, it should be noted that other nomenclatures do exist.[49−51] The regime that graft-copolymers belong to dictates how the crowding of side chains along the backbone affects the rigidity of the polymer, specifically the Kuhn length. The largest factors contributing to which regime bottlebrushes belong to are grafting density (n_g), side chain length (n_{sc}), and backbone/side-chain monomer volumes (v_b and v_s). Table 1 collects all of the necessary values to form graft-copolymer phase diagrams for our systems.[4,49,52,53]

Table 1. Collection of Architectural Parameters Associated with Poly(norbornene), Poly(methyl methacrylate), and Poly(dimethylsiloxane) (PNB, PMMA, and PDMS, Respectively)[a]

architectural parameter	PNB value	PMMA value	PDMS value
monomer length (l_b or l_s)	0.61 nm	0.25 nm	0.31 nm
Kuhn length (b_b or b_s)	1.70 nm	1.50 nm	1.30 nm
monomer volume ($v_b$or v_s)	0.20 nm^3	0.15 nm^3	0.13 nm^3
grafting density (n_g)	1 unit	1 unit	n/a

[a]The monomer volumes within Table 1 were calculated using $v = m(dN_A)^{-1}$, where m is the monomer mass, d is the monomer mass density, and N_A is Avagodro's number.

Using these parameters, two graft-copolymer phase diagrams were constructed for PNB-*g*-PDMS and PMMA-*g*-PDMS (Figure S.8), indicating that our ROMP and FRP samples belong to the SBB and SSC regimes, respectively. Given that norbornene has a larger v_b than methyl methacrylate (0.20 *vs* 0.15 nm^3), it is unsurprising that PNB-*g*-PDMS bottlebrushes belong to a less extended regime than PMMA-*g*-PDMS bottlebrushes. The flexibility of these systems is reflected in their effective Kuhn lengths of b_k = 2.15 and 2.80 nm for PNB-*g*-PDMS and PMMA-*g*-PDMS graft-copolymer bottlebrushes, respectively.

Following the SBB and SSC regime classifications, the elastic modulus (E_o) of the ROMP and FRP systems were modeled using Dobrynin and co-workers' adaptation of the affine model for the elasticity of BBEs[4]

$$E_o = 3Ck_bT\beta\alpha^{-1}\rho_s \quad (2)$$

where k_b is the Boltzmann constant, T is the absolute temperature, β is the strand-extension ratio, α is the strand stiffness, ρ_s is the number density of stress-supporting strands, and the scaling constant C = 1. For an affine bottlebrush network, the theoretical number density of stress-supporting strands is:[4,9]

$$\rho_s = \rho\varphi(n_x^{-1} - 2n_{bb}^{-1}) \quad (3)$$

where ρ is the monomer number density, n_{bb} is the degree of polymerization of the bottlebrush backbone, and φ is the volume fraction of backbone monomers. Though we required an affine model to model ideal BBEs, it should be noted that the elastic moduli of BBEs are better described by a phantom network model (Figure S.10).

Structural Efficiency Ratio. Analysis of eq 2 and 3 indicates that we can compare the measured elastic modulus to the physical and chemical properties of the network

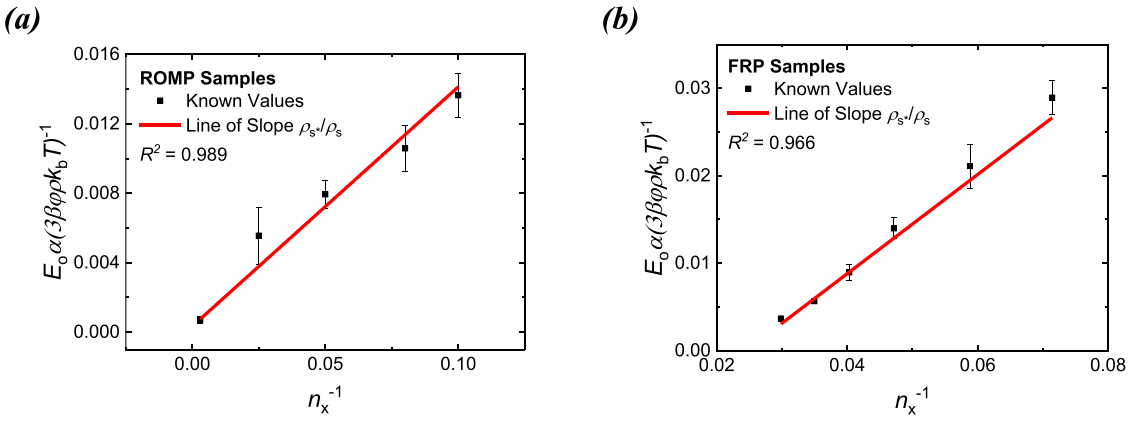

(c)

Parameter	ROMP	FRP	Sheiko, *et al.*
ρ_{s*}/ρ_s	0.14	0.57	0.26
ρ	5.00 nm^{-3}	6.67 nm^{-3}	6.67 nm^{-3}

Figure 4. Plots of n_x^{-1} against $E_o\alpha(3\beta\varphi\rho k_bT)^{-1}$ for our (a) ROMP and (b) FRP samples (refer to Figure S.11 for a plot of Sheiko et al.'s FRP samples), the slope of each line providing the value for the SER. (c) Collection of the SERs for our ROMP and FRP systems as well as Sheiko and co-workers' samples from ref 4. Note that our FRP was solventless and Sheiko and co-workers' FRP was performed in *p*-xylene. The E_o values used for Sheiko et al.'s FRP samples were obtained using eq S.1 and are tabulated in Table S.1.

https://doi.org/10.1021/acs.macromol.2c01332
Macromolecules 2022, 55, 10312−10319

components. The experimentally determined number density of stress-supporting strands (ρ_{s*}) will be lower than that predicted by the affine model (ρ_s) because not all monomers are part of stress-supporting strands, a typical scenario for viscoelastic systems. To estimate the degree of network defects, we introduce the concept of the structural efficiency ratio (SER = ρ_{s*}/ρ_s), a comparison between the number density of stress-supporting strands in an experimental network (ρ_{s*}) to that of an affine model network (ρ_s).

Due to the presence of molecular defects in our BBEs (or any network), it stands to reason that values of ρ_{s*} for our systems will be lower than the values of ρ_s for the most perfect, ideal cases. To quantify the differences between ρ_{s*} and ρ_s, we divide both sides of eq 2 by ρ_s and plot the known parameters of our network against one another as defined in eq 4:

$$\frac{\alpha E_o}{3\beta\varphi\rho k_b T} = \frac{\rho_{s*}}{\rho_s} n_x^{-1} - B_o \tag{4}$$

where B_o is a numerical constant defined by the line's y-intercept. To calculate the normalized y-axis, we use the monomer number density calculated by inverting the volume of a monomer, *e.g.*, norbornene carboxylic acid, with a monomer volume of 0.20 nm^3 and a monomer number density of 1/0.20 nm^3 = 5.00 nm^{-3}. The calculation of α, β, and φ are detailed by eqs S.6−S.12.

The slopes of the lines within Figure 4a,b represent the ratio ρ_{s*}/ρ_s for our ROMP and FRP samples and are tabulated in Figure 4c along with the corresponding value for Sheiko, et al.'s FRP samples. The SER provides insight into the efficiency of a given chemistry at forming stress-supporting strands, namely, the percentage of strands within a cubic nanometer that are stress-supporting (relative to the affine case). A physical interpretation of ρ_{s*}/ρ_s is illustrated in Figure 5, where red strands represent stress-supporting strands and black strands represent strands that should be stress-supporting but *are not* due to molecular defects within the BBE.

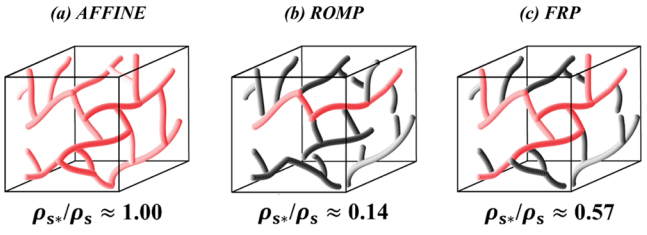

Figure 5. Representative depiction of 1 nm^3 sections of (a) an ideally formed, affine BBE, (b) a ROMP BBE, and (c) a solventless FRP BBE. The red strands represent stress-supporting strands, while the black strands represent strands that should be stress-supporting but are not due to molecular defects introduced to the network by the chemistry.

This ratio is useful when comparing the efficiency of BBEs polymerized under different conditions. For example, we would predict that Sheiko and co-workers' low-SER FRP samples ($\rho_{s*}/\rho_s \approx 0.26$) have fewer stress-supporting strands, more network defects, and lower E_o than our higher-SER FRP samples ($\rho_{s*}/\rho_s \approx 0.57$). Recalling that Sheiko and co-workers' system was polymerized in solvent, this observation is particularly interesting because it suggests that the presence of solvent has a large effect on the number of stress-supporting strands formed within the FRP networks. Indeed, experimentation with the conditions of our FRP led to samples that decreased in E_o as the weight percent of p-xylene increased (Figure 6). For example, the addition of solvent to the polymerization of an n_x = 14 BBE decreased E_o from ∼114 kPa to ∼45 kPa.

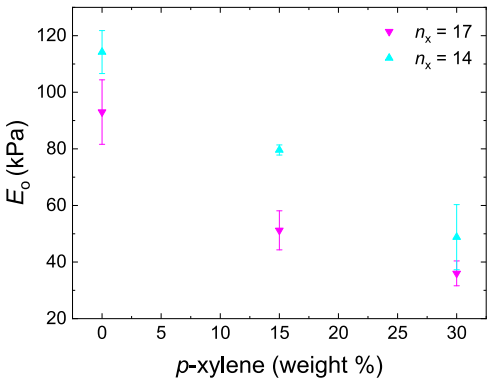

Figure 6. Plot of the quasi-elastic apparent modulus (E_o) measured in FRP samples prepared using various weight percentages of p-xylene as a solvent. Two n_x's of sample were investigated: n_x = 17 (magenta upside-down triangles) and n_x = 14 (cyan triangles). The data indicates that increasing the weight percent of solvent used leads to a decrease in the experimentally determined E_o values. All E_o measurements were taken at 0.01 Hz.

These results led us to conclude that the use of solvent in FRP allows for a lower SER and therefore fewer stress-supporting strands within each cubic nanometer of the BBEs. Furthermore, both Sheiko et al.'s BBEs and our ROMP BBEs were polymerized with solvent and are also capable of producing samples with much lower crosslink densities than our solventless FRP system (n_x > 333 *vs* n_x <40). This further implies that when the concentration of crosslinker is low, the presence of solvent is advantageous, allowing for crosslinkers to be used "more efficiently" than within a solventless system.

Additionally, based on the values of ρ_{s*}/ρ_s extracted from the model (Figure 4c), the efficiency of the ROMP chemistry ($\rho_{s*}/\rho_s \approx 0.14$) at producing stress-supporting strands is considerably lower than that of our FRP system ($\rho_{s*}/\rho_s \approx 0.57$). This implies that the large differences in elastic moduli seen at lower n_x values (higher crosslink densities) in Figure 3 are a result of the crosslinking becoming less efficient as the concentration of crosslinker is increased relative to the macromonomer. It is likely that the probability of successive crosslinkers being added to the "living" chain increases as the amount of crosslinker increases, resulting in networks where the number of stress-supporting strands is lower due to the increased number of ineffective crosslinks distributed throughout the network of the ROMP samples.

With this insight into network topology, it follows that the ROMP samples would have a larger number of molecular defects than the FRP samples and therefore would likely have a greater viscous component to their moduli (at low frequencies).[54] Through dynamic mechanical analysis (DMA) of our systems (Figure 7), we show that this observation is true, with ROMP samples always having higher loss moduli (Figure 7a,b) and loss tangents (Figure 7c) than similarly crosslinked FRP samples at low frequencies. The magnitude of the complex moduli (Figure 7d) for each of the BBEs follows the same trends depicted in Figure 3, showing how the ROMP samples are softer than FRP samples with

https://doi.org/10.1021/acs.macromol.2c01332
Macromolecules 2022, 55, 10312−10319

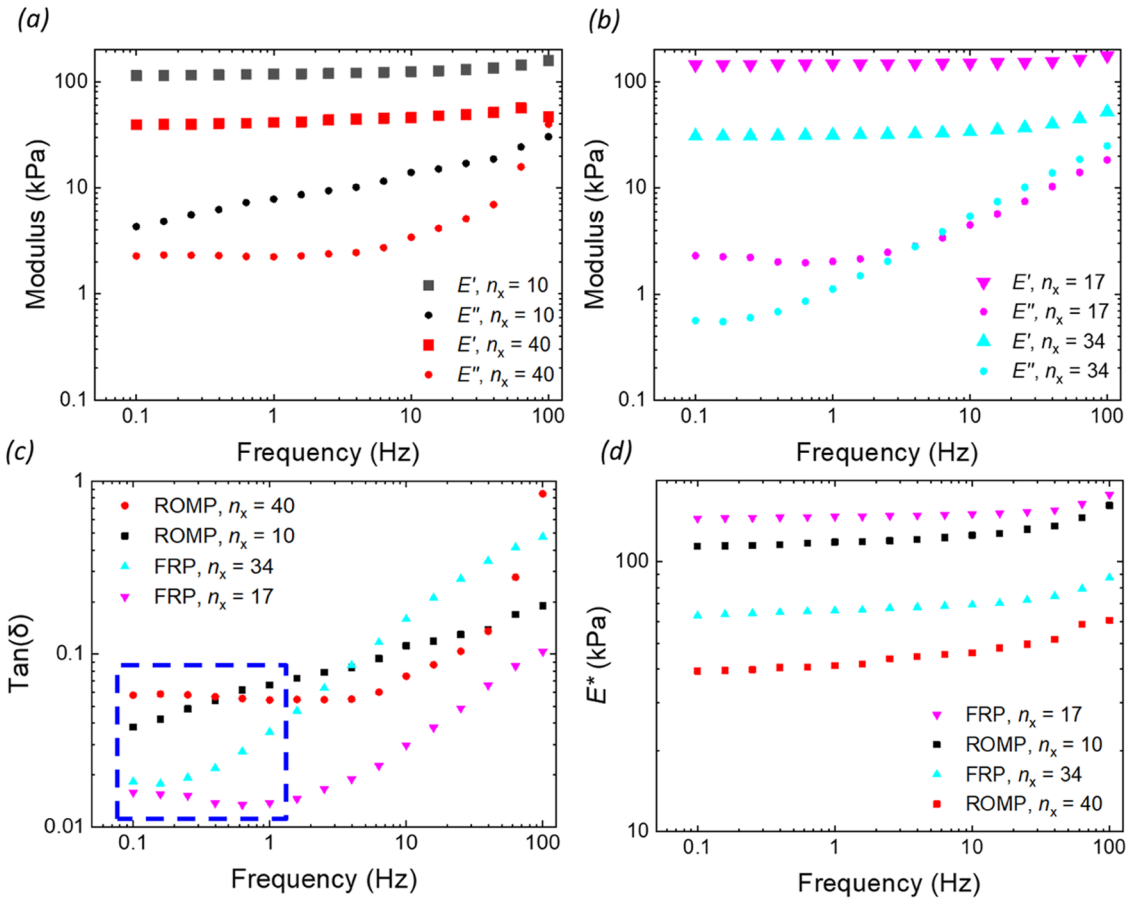

Figure 7. Dynamic mechanical analysis (DMA) of several ROMP and FRP samples. E^* and tan(δ) refer to the complex modulus and loss tangent respectively. The storage and loss moduli (E' and E'', respectively) of the ROMP (a) and FRP (b) samples illustrate how the magnitude of the loss moduli for ROMP samples is higher than that of similarly crosslinked FRP samples in the low-frequency regime (0.1−1 Hz). The loss tangents of the ROMP samples (c) are greater than that of the FRP samples within the low-frequency regime (as outlined by the blue box), indicating that the loss modulus has a higher contribution to the E^* in ROMP samples. This contribution can be seen in (d) a direct comparison between the E^* of the ROMP and FRP samples, where the ROMP samples always have lower E^* than analogously crosslinked FRP samples.

analogous amounts of crosslinker due to the increased number of molecular defects.

CONCLUSIONS

Herein, the efficiencies of the ROMP and FRP chemistries at producing stress-supporting strands are evaluated through the use of Dobrynin et al.'s affine model for BBE modulus. To facilitate this comparison, we introduce the concept of the structural efficiency ratio (SER = ρ_{s*}/ρ_s), a comparison of the number density of stress-supporting strands in a real BBE (ρ_{s*}) to the expected number density of stress-supporting strands for an affine system (ρ_s). This SER provides a quantitative measure of the relative number of molecular defects within each sample set, revealing that the ROMP chemistry produces stress-supporting strands much less efficiently than the FRP chemistry. The SER was additionally demonstrated to correctly predict (1) that the addition of solvent to FRP results in samples with lower E_o and (2) that ROMP samples had both higher loss moduli and loss tangents than similarly crosslinked FRP samples. This analysis using ρ_{s*}/ρ_s provides a unique and simple method by which it is possible to use chemistry as another "knob" to design materials using only theoretical information and knowledge of the elastic modulus.

ASSOCIATED CONTENT

Supporting Information

The Supporting Information is available free of charge at https://pubs.acs.org/doi/10.1021/acs.macromol.2c01332.

Synthesis, Mechanical Characterization, and Model (PDF)

AUTHOR INFORMATION

Corresponding Authors

Mark Ilton − *Department of Physics, Harvey Mudd College, Claremont, California 91711, United States*; Email: milton@g.hmc.edu

James J. Watkins − *Department of Polymer Science and Engineering, University of Massachusetts Amherst, Amherst, Massachusetts 01003, United States*; orcid.org/0000-0001-8302-825X; Email: watkins@polysci.umass.edu

Alfred J. Crosby − *Department of Polymer Science and Engineering, University of Massachusetts Amherst, Amherst, Massachusetts 01003, United States*; Email: crosby@mail.pse.umass.edu

Gregory N. Tew − *Department of Polymer Science and Engineering, University of Massachusetts Amherst, Amherst, Massachusetts 01003, United States*; orcid.org/0000-0003-3277-7925; Email: tew@mail.pse.umass.edu

https://doi.org/10.1021/acs.macromol.2c01332
Macromolecules 2022, 55, 10312−10319

Authors

Brandon R. Clarke − *Department of Polymer Science and Engineering, University of Massachusetts Amherst, Amherst, Massachusetts 01003, United States*

Hyemin Kim − *Department of Polymer Science and Engineering, University of Massachusetts Amherst, Amherst, Massachusetts 01003, United States*

Complete contact information is available at: https://pubs.acs.org/10.1021/acs.macromol.2c01332

Author Contributions

§B.R.C. and H.K. contributed equally to this work.

Notes

The authors declare no competing financial interest.

■ ACKNOWLEDGMENTS

This research was funded by the US Department of Education Graduate Assistance in Areas of Need (GAANN) Fellowship, the National Institute of Health (NIH) National Research Service Award T32 GM135096, and the Army Research Lab (ARL) Army Research Lab Award W911NF2120208. Facilities used during the conducting of this research are maintained by the University of Massachusetts, Amherst.

■ REFERENCES

(1) Xie, R.; Mukherjee, S.; Levi, A. E.; Reynolds, V. G.; Wang, H.; Chabinyc, M. L.; Bates, C. M. Room Temperature 3D Printing of Super-Soft and Solvent-Free Elastomers. *Sci. Adv.* **2020**, *6*, No. eabc6900.

(2) Clarke, B. R.; Tew, G. N. Synthesis and Characterization of Poly(Ethylene Glycol) Bottlebrush Networks via Ring-Opening Metathesis Polymerization. *J. Polym. Sci.* **2022**, *60*, 1501−1510.

(3) Xie, G.; Martinez, M. R.; Olszewski, M.; Sheiko, S. S.; Matyjaszewski, K. Molecular Bottlebrushes as Novel Materials. *Biomacromolecules* **2019**, *20*, 27−54.

(4) Vatankhah-Varnosfaderani, M.; Daniel, W. F. M.; Everhart, M. H.; Pandya, A. A.; Liang, H.; Matyjaszewski, K.; Dobrynin, A. V.; Sheiko, S. S. Mimicking Biological Stress-Strain Behaviour with Synthetic Elastomers. *Nature* **2017**, *549*, 497−501.

(5) Clarke, B. R.; Tew, G. N. Bottlebrush Amphiphilic Polymer Co-Networks. *Macromolecules* **2022**, *55*, 5131−5139.

(6) Cai, L. H.; Kodger, T. E.; Guerra, R. E.; Pegoraro, A. F.; Rubinstein, M.; Weitz, D. A. Soft Poly(Dimethylsiloxane) Elastomers from Architecture-Driven Entanglement Free Design. *Adv. Mater.* **2015**, *27*, 5132−5140.

(7) Daniel, W. F. M.; Burdyńska, J.; Vatankhah-Varnoosfaderani, M.; Matyjaszewski, K.; Paturej, J.; Rubinstein, M.; Dobrynin, A. V.; Sheiko, S. S. Solvent-Free, Supersoft and Superelastic Bottlebrush Melts and Networks. *Nat. Mater.* **2016**, *15*, 183−189.

(8) Mukherjee, S.; Xie, R.; Reynolds, V. G.; Uchiyama, T.; Levi, A. E.; Valois, E.; Wang, H.; Chabinyc, M. L.; Bates, C. M. Universal Approach to Photo-Crosslink Bottlebrush Polymers. *Macromolecules* **2020**, *53*, 1090−1097.

(9) Sheiko, S. S.; Dobrynin, A. V. Architectural Code for Rubber Elasticity: From Supersoft to Superfirm Materials. *Macromolecules* **2019**, *52*, 7531−7546.

(10) Sarapas, J. M.; Chan, E. P.; Rettner, E. M.; Beers, K. L. Compressing and Swelling to Study the Structure of Extremely Soft Bottlebrush Networks Prepared by ROMP. *Macromolecules* **2018**, *51*, 2359−2366.

(11) Cao, Z.; Daniel, W. F. M.; Vatankhah-Varnosfaderani, M.; Sheiko, S. S.; Dobrynin, A. V. Dynamics of Bottlebrush Networks. *Macromolecules* **2016**, *49*, 8009−8017.

(12) Cushman, K.; Keith, A.; Tanaka, J.; Sheiko, S. S.; You, W. Investigating the Stress-Strain Behavior in Ring-Opening Metathesis Polymerization-Based Brush Elastomers. *Macromolecules* **2021**, *54*, 8365−8371.

(13) Li, Z.; Tang, M.; Liang, S.; Zhang, M.; Biesold, G. M.; He, Y.; Hao, S. M.; Choi, W.; Liu, Y.; Peng, J.; Lin, Z. Bottlebrush Polymers: From Controlled Synthesis, Self-Assembly, Properties to Applications. *Prog. Polym. Sci.* **2021**, *116*, No. 101387.

(14) Weaver, J. A.; Morelly, S. L.; Alvarez, N. J.; Magenau, A. J. D. Grafting-through ROMP for Gels with Tailorable Moduli and Crosslink Densities. *Polym. Chem.* **2018**, *9*, 5173−5178.

(15) Keith, A. N.; Clair, C.; Lallam, A.; Bersenev, E. A.; Ivanov, D. A.; Tian, Y.; Dobrynin, A. V.; Sheiko, S. S. Independently Tuning Elastomer Softness and Firmness by Incorporating Side Chain Mixtures into Bottlebrush Network Strands. *Macromolecules* **2020**, *53*, 9306−9312.

(16) Keith, A. N.; Vatankhah-Varnosfaderani, M.; Clair, C.; Fahimipour, F.; Dashtimoghadam, E.; Lallam, A.; Sztucki, M.; Ivanov, D. A.; Liang, H.; Dobrynin, A. V.; Sheiko, S. S. Bottlebrush Bridge between Soft Gels and Firm Tissues. *ACS Cent. Sci.* **2020**, *6*, 413−419.

(17) Liang, H.; Sheiko, S. S.; Dobrynin, A. V. Supersoft and Hyperelastic Polymer Networks with Brushlike Strands. *Macromolecules* **2018**, *51*, 638−645.

(18) Aoyama, T.; Yamada, N.; Urayama, K. Nonlinear Elasticity of Ultrasoft Near-Critical Gels with Extremely Sparse Network Structures Revealed by Biaxial Stretching. *Macromolecules* **2021**, *54*, 2353−2365.

(19) Jacobs, M.; Liang, H.; Dashtimoghadam, E.; Morgan, B. J.; Sheiko, S. S.; Dobrynin, A. V. Nonlinear Elasticity and Swelling of Comb and Bottlebrush Networks. *Macromolecules* **2019**, *52*, 5095−5101.

(20) Tian, Y.; Ina, M.; Cao, Z.; Sheiko, S. S.; Dobrynin, A. V. How to Measure Work of Adhesion and Surface Tension of Soft Polymeric Materials. *Macromolecules* **2018**, *51*, 4059−4067.

(21) Creton, C.; Ciccotti, M. Fracture and Adhesion of Soft Materials: A Review. *Reports Prog. Phys.* **2016**, *79*, No. 046601.

(22) Panyukov, S. Theory of Flexible Polymer Networks: Elasticity and Heterogeneities. *Polymers* **2020**, *12*, No. 767.

(23) Barney, C. W.; Dougan, C. E.; McLeod, K. R.; Kazemi-Moridani, A.; Zheng, Y.; Ye, Z.; Tiwari, S.; Sacligil, I.; Riggleman, R. A.; Cai, S.; et al. Cavitation in Soft Matter. *Proc. Natl. Acad. Sci. U.S.A.* **2020**, *117*, 9157−9165.

(24) Barney, C. W.; Zheng, Y.; Wu, S.; Cai, S.; Crosby, A. J. Residual Strain Effects in Needle-Induced Cavitation. *Soft Matter* **2019**, *15*, 7390−7397.

(25) Zhong, M.; Wang, R.; Kawamoto, K.; Olsen, B. D.; Johnson, J. A. Quantifying the Impact of Molecular Defects on Polymer Network Elasticity. *Science* **2016**, *353*, 1264−1268.

(26) Akagi, Y.; Gong, J. P.; Chung, U.-i.; Sakai, T. Transition between Phantom and Affine Network Model Observed in Polymer Gels with Controlled Network Structure. *Macromolecules* **2013**, *46*, 1035−1040.

(27) Barney, C. W.; Ye, Z.; Sacligil, I.; McLeod, K. R.; Zhang, H.; Tew, G. N.; Riggleman, R. A.; Crosby, A. J. Fracture of Model End-Linked Networks. *Proc. Natl. Acad. Sci. U.S.A.* **2022**, *119*, No. e2112389119.

(28) Tiwari, S.; Kazemi-Moridani, A.; Zheng, Y.; Barney, C. W.; McLeod, K. R.; Dougan, C. E.; Crosby, A. J.; Tew, G. N.; Peyton, S. R.; Cai, S.; Lee, J. H. Seeded Laser-Induced Cavitation for Studying High-Strain-Rate Irreversible Deformation of Soft Materials. *Soft Matter* **2020**, *16*, 9006−9013.

(29) Kim, J.; Zhang, G.; Shi, M.; Suo, Z. Fracture, Fatigue, and Friction of Polymers in Which Entanglements Greatly Outnumber Cross-Links. *Science* **2021**, *374*, 212−216.

(30) Cao, Z.; Carrillo, J. M. Y.; Sheiko, S. S.; Dobrynin, A. V. Computer Simulations of Bottle Brushes: From Melts to Soft Networks. *Macromolecules* **2015**, *48*, 5006−5015.

(31) Hatami-Marbini, H. Effect of Crosslink Torsional Stiffness on Elastic Behavior of Semiflexible Polymer Networks. *Phys. Rev. E* **2018**, *97*, 1−6.

(32) Golitsyn, Y.; Pulst, M.; Samiullah, M. H.; Busse, K.; Kressler, J.; Reichert, D. Crystallization in PEG Networks: The Importance of Network Topology and Chain Tilt in Crystals. *Polymer* **2019**, *165*, 72−82.
(33) Kawamoto, K.; Zhong, M.; Wang, R.; Olsen, B. D.; Johnson, J. A. Loops versus Branch Functionality in Model Click Hydrogels. *Macromolecules* **2015**, *48*, 8980−8988.
(34) Sorichetti, V.; Ninarello, A.; Ruiz-Franco, J. M.; Hugouvieux, V.; Kob, W.; Zaccarelli, E.; Rovigatti, L. Effect of Chain Polydispersity on the Elasticity of Disordered Polymer Networks. *Macromolecules* **2021**, *54*, 3769−3779.
(35) Ngai, K. L.; Roland, C. M. Junction Dynamics and the Elasticity of Networks. *Macromolecules* **1994**, *27*, 2454−2459.
(36) Fujiyabu, T.; Yoshikawa, Y.; Chung, U.; il Sakai, T. Structure-Property Relationship of a Model Network Containing Solvent. *Sci. Technol. Adv. Mater.* **2019**, *20*, 608−621.
(37) Chan, D.; Ding, Y.; Dauskardt, R. H.; Appel, E. A. Engineering the Mechanical Properties of Polymer Networks with Precise Doping of Primary Defects. *ACS Appl. Mater. Interfaces* **2017**, *9*, 42217−42224.
(38) Lin, T. S.; Wang, R.; Johnson, J. A.; Olsen, B. D. Revisiting the Elasticity Theory for Real Gaussian Phantom Networks. *Macromolecules* **2019**, *52*, 1685−1694.
(39) Lang, M. Elasticity of Phantom Model Networks with Cyclic Defects. *ACS Macro Lett.* **2018**, *7*, 536−539.
(40) Lin, T. S.; Wang, R.; Johnson, J. A.; Olsen, B. D. Extending the Phantom Network Theory to Account for Cooperative Effect of Defects. *Macromol. Symp.* **2019**, *385*, No. 1900010.
(41) Fu, L.; Li, H. Toward Quantitative Prediction of the Mechanical Properties of Tandem Modular Elastomeric Protein-Based Hydrogels. *Macromolecules* **2020**, *53*, 4704−4710.
(42) Odian, G. *Principles of Polymerization*, 4th ed.; John Wiley & Sons, Ltd.: Hoboken, NJ, 2004.
(43) Radzinski, S. C.; Foster, J. C.; Chapleski, R. C.; Troya, D.; Matson, J. B. Bottlebrush Polymer Synthesis by Ring-Opening Metathesis Polymerization: The Significance of the Anchor Group. *J. Am. Chem. Soc.* **2016**, *138*, 6998−7004.
(44) Beuermann, S.; Harrisson, S.; Hutchinson, R. A.; Junkers, T.; Russell, G. T. Update and Critical Reanalysis of IUPAC Benchmark Propagation Rate Coefficient Data. *Polym. Chem.* **2022**, *13*, 1891−1900.
(45) Shull, K. R.; Ahn, D.; Chen, W.-L.; Flanigan, C. M.; Crosby; Alfred, J. Axisymmetric Adhesion Tests of Soft Materials. *Macromol. Chem. Phys.* **1998**, 489−511.
(46) Liang, H.; Morgan, B. J.; Xie, G.; Martinez, M. R.; Zhulina, E. B.; Matyjaszewski, K.; Sheiko, S. S.; Dobrynin, A. V. Universality of the Entanglement Plateau Modulus of Comb and Bottlebrush Polymer Melts. *Macromolecules* **2018**, *51*, 10028−10039.
(47) Vatankhah-Varnoosfaderani, M.; Daniel, W. F. M.; Zhushma, A. P.; Li, Q.; Morgan, B. J.; Matyjaszewski, K.; Armstrong, D. P.; Spontak, R. J.; Dobrynin, A. V.; Sheiko, S. S. Bottlebrush Elastomers: A New Platform for Freestanding Electroactuation. *Adv. Mater.* **2017**, *29*, No. 1604209.
(48) Rubinstein, M.; Colby, R. H. *Polymer Physics*, 2nd ed.; Oxford University Press: Oxford, New York, 2003.
(49) Liang, H.; Wang, Z.; Sheiko, S. S.; Dobrynin, A. V. Comb and Bottlebrush Graft Copolymers in a Melt. *Macromolecules* **2019**, *52*, 3942−3950.
(50) Cai, L. H. Molecular Understanding for Large Deformations of Soft Bottlebrush Polymer Networks. *Soft Matter* **2020**, *16*, 6259−6264.
(51) Paturej, J.; Sheiko, S. S.; Panyukov, S.; Rubinstein, M. Molecular Structure of Bottlebrush Polymers in Melts. *Sci. Adv.* **2016**, *2*, No. 1601478.
(52) Crow. Kuhn and Persistence Length of Polymers. http://polymerdatabase.com/polymerphysics/lpTable.html.
(53) Mark, J. E. *Physical Properties of Polymers*, 2nd ed.; Springer Science+Business Media, LLC: New York, NY, 2007, DOI: 10.1007/BF01840027.
(54) Ferry, J. *Viscoelastic Properties of Polymers*; John Wiley & Sons, 1980.

https://doi.org/10.1021/acs.macromol.2c01332
Macromolecules 2022, 55, 10312−10319